Engineering Structures 93 (2015) 27–35

Contents lists available at ScienceDirect

Engineering Structures

journal homepage: www.elsevier.com/locate/engstruct

Shape optimization of U-shaped damper for improving its bi-directional performance under cyclic loading

Kailai Deng [a], Peng Pan [b,*], Yukun Su [a], Yantao Xue [c]

[a] Department of Civil Engineering, Tsinghua University, Beijing 100084, China
[b] Key Laboratory of Civil Engineering Safety and Durability of China Education Ministry, Department of Civil Engineering, Tsinghua University, Beijing 100084, China
[c] Institute of Building Structures, China Academy of Building Research, Beijing 100013, China

ARTICLE INFO

Article history:
Received 19 January 2014
Revised 28 February 2015
Accepted 2 March 2015
Available online 23 March 2015

Keywords:
U-shaped damper
Bi-directional performance
Shape optimization
Response surface method

ABSTRACT

A U-shaped damper typically has a stable and saturated hysteretic performance along the in-plane direction and is usually installed in the isolation layer. However experimental study shows that the conventional U-shaped damper presents an unstable hysteretic performance when it sustains bi-directional deformations. Therefore, shape optimization is needed to improve the hysteretic performance of the U-shaped damper. To obtain an optimal shape for the U-shaped damper, a finite element (FE) model was built using a general FE analysis software called ABAQUS. Comparisons of results obtained from FE models with those obtained from experimental studies demonstrated the effectiveness of the FE models. Optimization of a U-shaped damper was carried out using the FE model. The length and shape of the straight part of the U-shaped damper were treated as optimization parameters and the enlarging the end of the straight part was adopted as the improved approach. The formula for the ratio of the energy dissipated by rate-independent and rate-dependent plastic deformation (*ALLPD*) to the maximum cumulative equivalent plastic strain (*PEEQ*) was derived though regression analysis. After four levels of optimization processes the optimal shape of the improved U-shaped damper was obtained, and the bi-directional performance was significantly improved compared to that of a conventional U-shaped damper.

1. Introduction

In seismic design the hysteresis damper has stable performance and good economy and is widely used in the seismic design of buildings and bridges [1–7]. Among these hysteretic dampers, the U-shaped damper shown in Fig. 1 has a stable restoring force and an extremely large deformation capacity. U-shaped dampers are often installed together with isolation bearings in building and bridge engineering [8].

Shaking table tests and time history analyses showed that a U-shaped damper can dissipate a consistent amount of energy and protect isolated structures from significant damage during earthquakes [9,10]. Isolation bearings in a building structure may sustain bi-directional deformation and this requires a damper to be installed in the isolation layer giving a stable performance when sustaining bi-directional deformation.

Many improved configurations of U-shaped dampers have been proposed. Kato and Kim proposed a complex mechanism to release the out-of-plane deformation of a U-shaped damper [11]. The parametric analysis of the damper was conducted with finite element analysis. The formula for the restoring force of the U-shaped damper was derived. Deng et al. developed a crawler damper for a bridge by adding two connecting plates to the U-shaped damper to control the deformation pattern of the energy dissipation plate [12]. A physical test and finite element analysis proved the effectiveness of the constraint from the connecting plate and a quantitative design method was established. A UH damper installed in the isolation layer was proposed based on a conventional U-shaped damper [13]. The results from the shaking table test proved the UH damper could protect the superstructure from significant damage during earthquakes. Other improved dampers based on the conventional U-shaped dampers have also been proposed in recent years [14–16]. As mentioned above, the bi-directional performance of the U-shaped damper needs to be extensively investigated when it is provided in the isolation layer. However, in existing studies the bi-directional performance of U-shaped damper under large amplitude cyclic loading has not been investigated.

However, with the development of computer technology and numerical analysis methods, the behavior of the structure can be

* Corresponding author. Tel.: +86 10 62794729; fax: +86 10 62788620.
E-mail address: panpeng@mail.tsinghua.edu.cn (P. Pan).

http://dx.doi.org/10.1016/j.engstruct.2015.03.006
0141-0296/

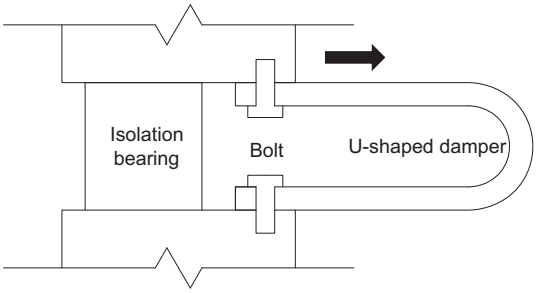

Fig. 1. U-shaped damper.

simulated using sophisticated finite element models [17,18], and optimized using advanced optimization techniques, e.g., genetic algorithms, simulated annealing algorithms and multi-level multi-disciplinary methods [19–22].

This study focused on the optimization of the bi-directional performance of a U-shaped damper. An experimental study was first carried out demonstrating the unstable bi-directional hysteretic performance of a conventional U-shaped damper. The concentration of the plastic strain leads to poor low cycle fatigue performance of the U-shaped damper under bi-directional loading. In order to optimize the response of U-shaped dampers under bi-directional loadings the geometry of the straight part of the damper has been changed by varying its width. To obtain the optimal shape parameters, a finite element method (FEM) was adopted as the optimization approach. The comparisons between the FEM simulation and test results demonstrated the effectiveness of the FEM. Finally, the shape optimization process was conducted and the length and width of the straight part of the U-shaped damper were adopted as the optimization parameters. The object of the optimization process was to maximize the energy dissipation capacity and minimize the equivalent plastic strain. After four optimization processes the optimal design parameters of the improved U-shaped damper were derived.

2. Estimation of strength

The U-shaped damper, which consists of two straight parts and one half-circle part, is shown in Fig. 2(a). The damper has four important shape parameters, the height (H), thickness (t) and width (w) of the U-shaped plate as well as the length of the straight part (l) of the damper. The radius of the half-circle part R is equal to $(H-t)/2$. The bi-directional behavior can be decomposed into two independent directions, i.e. the in-plane and out-of-plane. The in-plane deformation pattern of the U-shaped damper is shown in Fig. 2(b), and the in-plane strength F_{in} can be estimated as Eq. (1). Where, f_u is the ultimate strength of steel [12].

$$F_{in} = f_u \frac{t^2 w}{4R} \tag{1}$$

Fig. 2(c) presents the out-of-plane deformation pattern of the U-shaped damper. The out-of-plane strength F_{out} can be estimated as Eq. (2). Where, Q is the torsion resistance coefficient of the cross-section, and D_{out} is the out-of-plane deformation.

$$F_{\text{out}} = \frac{f_u\left(tw^2/2 + Q/\sqrt{3}\right)}{(l+R)\sqrt{4 - D_{\text{out}}^2/(l+R)^2}} \tag{2}$$

The strength of the U-shaped damper along the direction of α angle (Fig. 3(a)) can be estimated as Eq. (3).

$$F = F_{in}\cos\alpha + F_{\text{out}}\sin\alpha \tag{3}$$

3. Experimental study

3.1. Experimental plan

There were four specimens made of low yield point steel (LYP225) in the experiment study, as shown in Table 1. S1 was the standard specimen. S2's plate had a changed width at 20 mm. S3 and S4 had straight parts of 100 mm and 300 mm, respectively. The loading setup is shown in Fig. 3(b). The installation angle of the specimens is 45°. The ends of straight part are fixed on the loading frame through high-strength bolts, which can be taken as the fixed constraint. According to the current Chinese engineering practice, the maximum deformation demand of the damper is commonly between 200 mm and 300 mm, and the damper is required to sustain 30 cycles of loading for the maximum deformation demand. All the specimens were first loaded to an amplitude of 50 mm over two cycles, an amplitude of 100 mm over two cycles, an amplitude of 200 mm over thirty cycles, and finally an amplitude of 300 mm with multiple cycles until failure occurred. The loading scheme is shown in Fig. 4(a). The restoring force and shear deformation were measured by the load cell of the actuator and an external displacement transducer respectively, shown in Fig. 4(b).

3.2. Experimental results

Fig. 5 shows the hysteresis curves of the four specimens. The maximum restoring force for the 1st cycle of loading with the amplitude of 100 mm is adopted to validate the accuracy of the strength estimation. According to coupon test, the yield strength and ultimate strength of the steel are 202 MPa and 301 MPa, respectively. Table 2 presents the comparison between the analytical estimation and test results. It can be observed that Eq. (3) overestimates the restoring force for all the specimens, especially for S3 and S4. This is mainly because that Eq. (3) assumes a completely yield of the cross-sections, whereas the cross-sections are only partially yield and do not reach their ultimate strength in the physical tests. In addition, because of

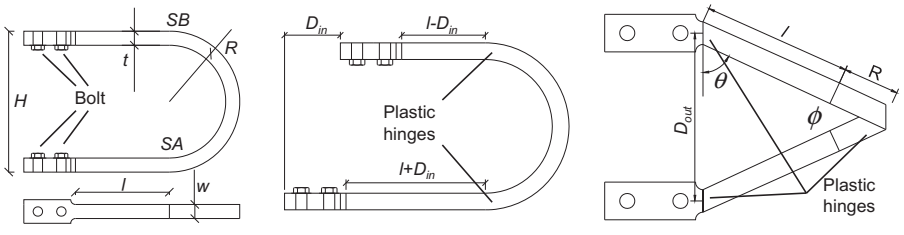

(a) Shape parameters (b) In-plane deformation (c) Out-of-plane deformation

Fig. 2. Parameters and deformation pattern of U-shaped damper.

Table 1
Details of specimens.

No.	t/mm	b/mm	l/mm	H/mm	Remarks
S1	30	30	200	300	Standard
S2	30	20	200	300	Smaller width
S3	30	30	100	300	Shorter straight part
S4	30	30	300	300	Longer straight part

the short straight part, the half-circle part of S3 sustains an obvious tensile deformation as shown in Fig. 6(a). The tensile deformation is not consisted with the assumed out-of-plane deformation, resulting a large error in strength estimation.

As the loading progressed, residual deformation appeared in the straight part of S1. The half-circle part of the damper turned in an orthogonal direction to the loading direction. After six cycles of loading at an amplitude of 200 mm there was no further increase in the residual deformation. The ultimate deformation mode of S1 is shown in Fig. 6(b). The damper presented a strong geometric nonlinearity while sustaining the bi-directional loading. Because of the geometric nonlinearity the restoring force of S1 was not stable. As shown in Fig. 5 the hysteresis curve of S1, S2 and S4 clearly decreased in the first six cycles of loading at an amplitude of 200 mm. Compared to the other specimen, S3 has a much shorter straight part. The half-circle part of S3 sustained significant tensile deformation when it was loaded to 200 mm. Therefore, S3 experienced less early strength degradation but failed relatively early. The failure modes of S3 and S1 are presented in Fig. 6(c) and (d), respectively. For the four specimens, the end of the straight part cracked finally. Large plastic strain was concentrated at the end of the straight part, leading to low cycle fatigue damage. Table 2 compares the fatigue performances of the same specimens in bi-directional tests with those obtained in out-of-plane unidirectional tests. The low cycle fatigue performances of the U-shaped damper for the bi-directional deformation is much worse than those for the out-of-plane unidirectional deformation.

4. Finite element model

For further study finite element analyses were conducted. The numerical model of the U-shaped damper is shown in Fig. 7, and was built using ABAQUS, a general FE software package. ABAQUS provides a constitutive model to describe the behavior of metal material under cyclic loading [23]. The kinematic hardening stress was calculated using Eq. (4). The relationship of the kinematic hardening stress to equivalent plastic strain (*PEEQ*) in this study is shown in Fig. 8. In ABAQUS, *PEEQ* is calculated as Eq. (5). The Von Mises yield criterion is employed and $\dot{\varepsilon}^{pl}$ is the plastic strain tensor rate. In this paper three backstresses are used to present the hardening effects of the steel material with large plastic strain. The parameters in the steel material constitutive model are shown in Fig. 8. Note that the material constitutive model could not simulate the failure of the steel material. The U-shaped plate was simulated with an 8-node, reducing integration with an hourglass, controlled linear brick element (C3D8R).

$$\alpha = \sum_{k=1}^{n} \frac{C_k}{\gamma_k}(1 - e^{-\gamma_k \bar{\varepsilon}^{pl}}) \tag{4}$$

$$\bar{\varepsilon}^{pl} = \int_0^t \sqrt{\frac{2}{3}\dot{\varepsilon}^{pl} : \dot{\varepsilon}^{pl}}\, dt \tag{5}$$

The loading scheme in FE analyses was similar to that in the physical test. It was found that residual deformation of the specimens did not increase, and the hysteresis curve became converged after 6 cycles of loading over 200 mm amplitude. The model was first loaded to an amplitude of 50 mm over two cycles, then to an amplitude of 100 mm over two cycles, then to an amplitude of 200 mm over six cycles, and finally to an amplitude of 300 mm over two cycles. For S3, since it was not loaded with the amplitude of 300 mm in the physical test, the simulation was also interrupted after 6 cycles of loading over the amplitude of 200 mm.

The hysteresis curves obtained from the finite element analyses are compared with those obtained from the test results in Fig. 9. The simulation well reproduces the degradation of the restoring force. The *ALLPD*, which represents the energy dissipated plastic deformation, in ABAQUS is calculated as Eq. (6). Where, σ is the stress tensor. The *ALLPDs* obtained in the numerical simulation and physical test are presented in Table 3. It can be observed that the error between the simulation and test results was no more than 10% for *ALLPD*, demonstrating the effectiveness of the numerical model.

$$ALLPD = \int_V \int_0^t \sigma : \dot{\varepsilon}^{pl} dt dv \tag{6}$$

According to previous research the low cycle fatigue performance had the relationship with the largest plastic strain as shown in Eq. (7) [24–26]. *Num* is the number of cycles corresponding to the largest plastic strain (ε) per cycle. Based on previous research the coefficient β for LYP225 steel usually equals about −0.6 [27,28].

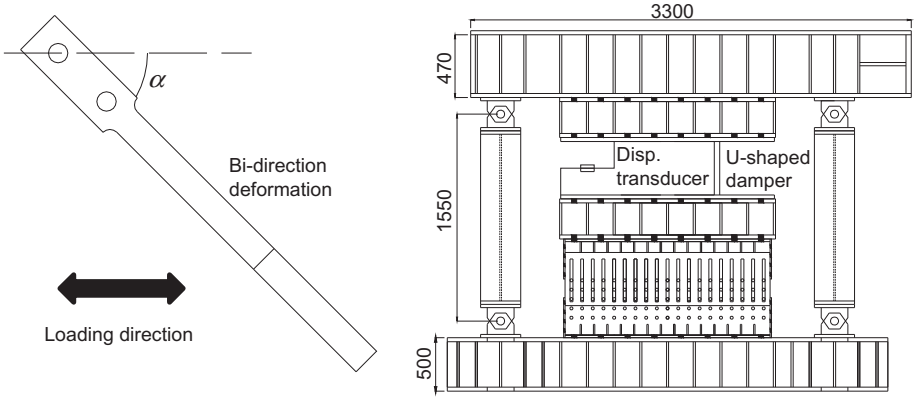

(a) Deformation direction (b) Loading setup

Fig. 3. Deformation direction and loading setup.

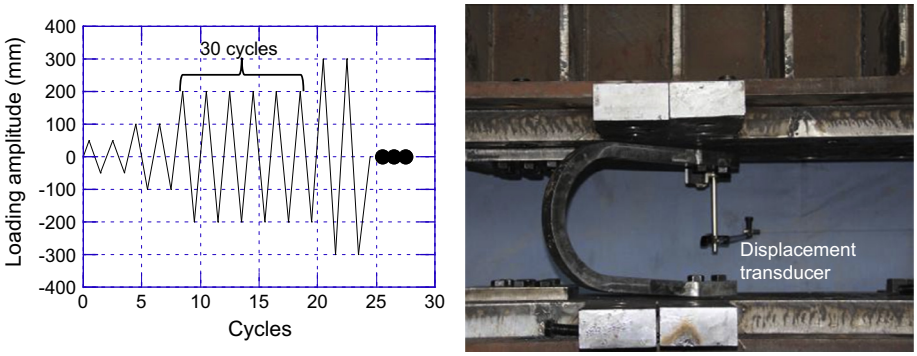

(a) Loading scheme (b) Displacement transducer

Fig. 4. Loading scheme and measurement.

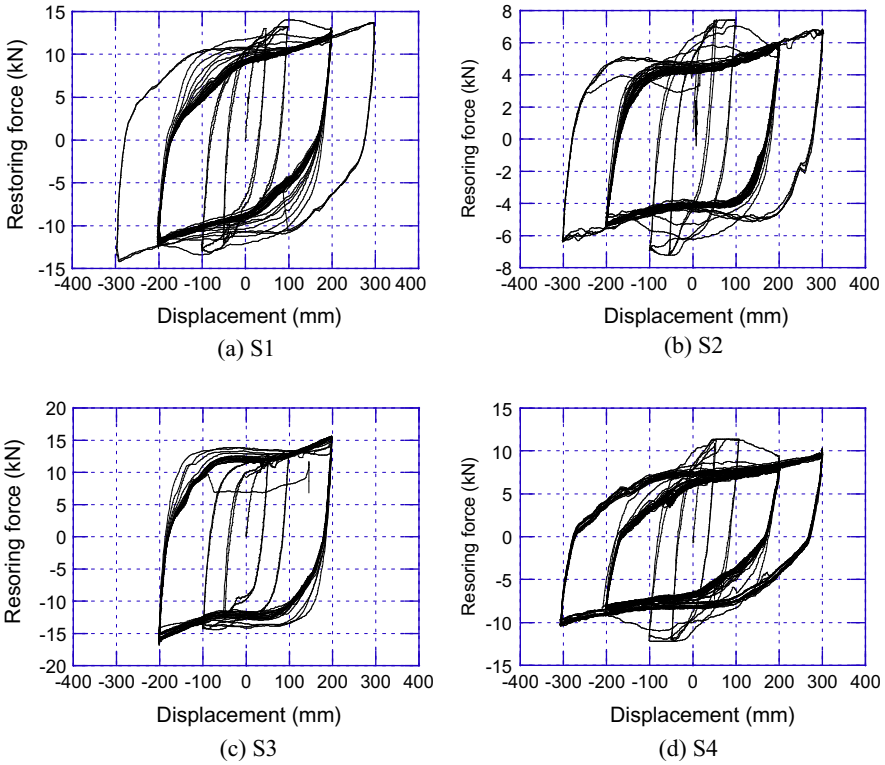

(a) S1 (b) S2

(c) S3 (d) S4

Fig. 5. Hysteresis curves of all the specimens.

Table 2
Experiment results.

No.	Eq. (6) (kN)	Test (kN)	Relative error (%)	Bi-direction test failure cycle	Out-of plane unidirectional test failure cycle
S1	16.92	13.40	26.29	3th of 300 mm	36th of 300 mm
S2	10.11	7.40	36.66	4th of 300 mm	48th of 300 mm
S3	20.13	13.10	53.67	18th of 200 mm	2nd of 300 mm
S4	15.44	11.20	37.82	15th of 300 mm	40th of 300 mm

Table 3 also compares the maximum *PEEQ* of the four finite element model under bi-directional and out-of-plane unidirectional deformation. It is found that the maximum *PEEQ* of the U-shaped damper under bi-directional deformation is 1.09–1.67 times of that under out-of-plane unidirectional deformation. In addition, combining the fatigue performance shown in Table 2, the results suggest that the maximum *PEEQ* is negatively proportional to the low cycle fatigue performance. Because the *PEEQ* was proportional to the largest plastic strain (ε) per cycle for the load scheme given in the "Finite element model" section, the maximum *PEEQ* were used in this study, meaning that the low cycle performance was proportional to $PEEQ_{\max}^{-0.6}$.

$$Num = \alpha\varepsilon^{\beta} \tag{7}$$

As shown in Fig. 10 the distribution of *PEEQ* for S1 concentrates on the end of straight part which leads to the unstable restoring force. The optimal design was to decrease the maximum *PEEQ* while not reducing the *ALLPD* significantly. So maximizing the $ALLPD/PEEQ_{\max}^{0.6}$, indicating the total energy dissipation capacity, was the objective of the optimization process.

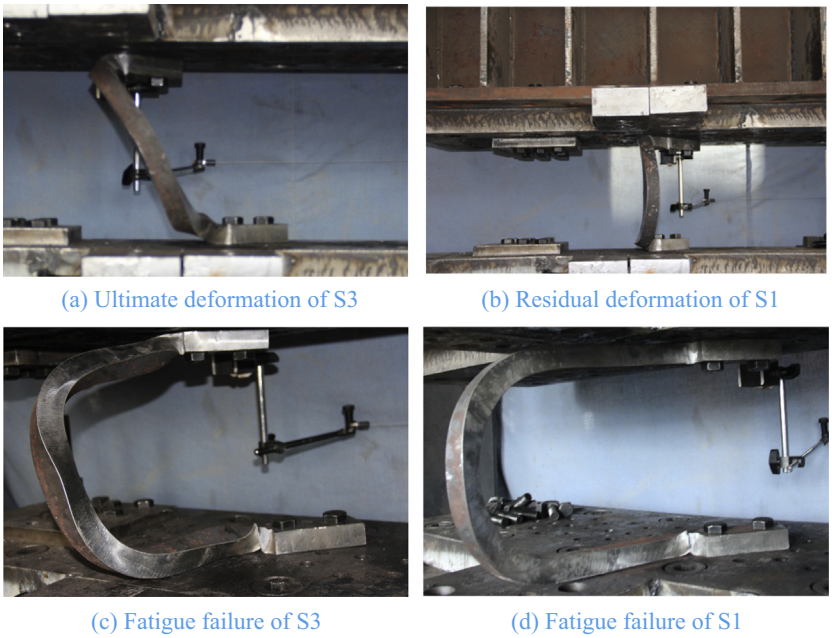

(a) Ultimate deformation of S3 (b) Residual deformation of S1

(c) Fatigue failure of S3 (d) Fatigue failure of S1

Fig. 6. Deformation and failure mode of the specimens.

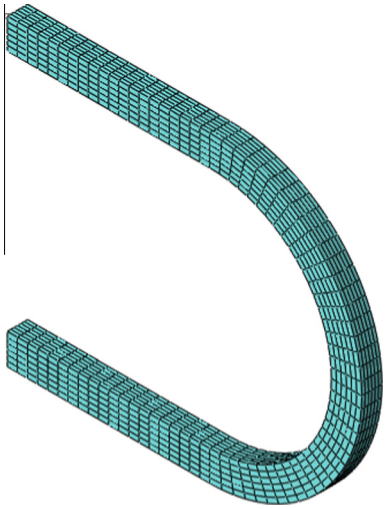

Fig. 7. Finite element model of U-shaped damper.

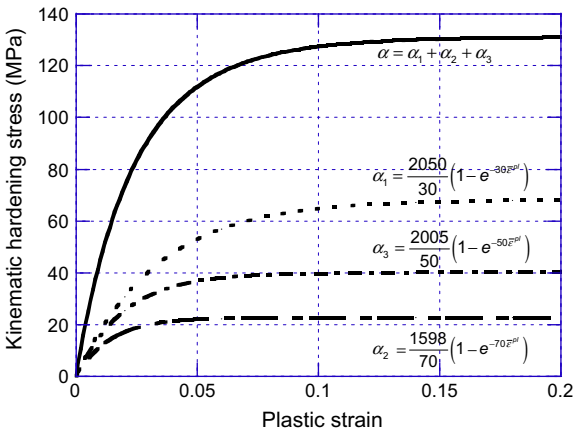

Fig. 8. Constitutive model for mental material.

5. Shape optimization

5.1. Optimization principle

According to the experimental study the end of the straight part should be strengthened to avoid the concentration of plastic strain and unrecoverable deformation of the U-shaped damper. In this study the optimization approaches proposed are shown in Fig. 11. To strengthen the U-shaped damper the end of the straight part in which b_2 represents its width, was enlarged. In the following optimization process the length of the straight part (l), and b_2, were adopted as the design parameters. The *ALLPD* and maximum *PEEQ* are the functions of l and b_2 under the determined loading scheme. The objective function of the optimization process is shown as Eq. (8).

$$\begin{cases} \text{Design variables} & l, b_2 \\ \text{Maximize} & ALLPD/PEEQ^{0.6}_{\max} \end{cases} \tag{8}$$

5.2. Optimization method

Because of the strong nonlinearity presented by the damper the analytical solution for the response was difficult to derive. The response surface method was adopted in this situation. The flowchart for the optimization process is shown in Fig. 12. Primary design parameters were determined first as shown in Table 4. The finite element (FE) analyses were also conducted using ABAQUS. In the analyses, the material constitutive model, and element type and size are the same with those adopted in Section 4, whose effectiveness has been validated. According to the results of the finite element analyses the response surfaces of *ALLPD* and maximum *PEEQ* were derived. The quadratic Pascal triangle polynomial as shown in Eq. (9) was used as the regression equation, where Z is the response, and x and y the variables. $a_{i,j}$ are the coefficients to be determined. In this case the response was $ALLPD/PEEQ^{0.6}_{\max}$, and the design variables were l and b_2.

$$Z = \sum_{0 \leqslant i,j \leqslant 2} a_{ij} x^i y^j \tag{9}$$

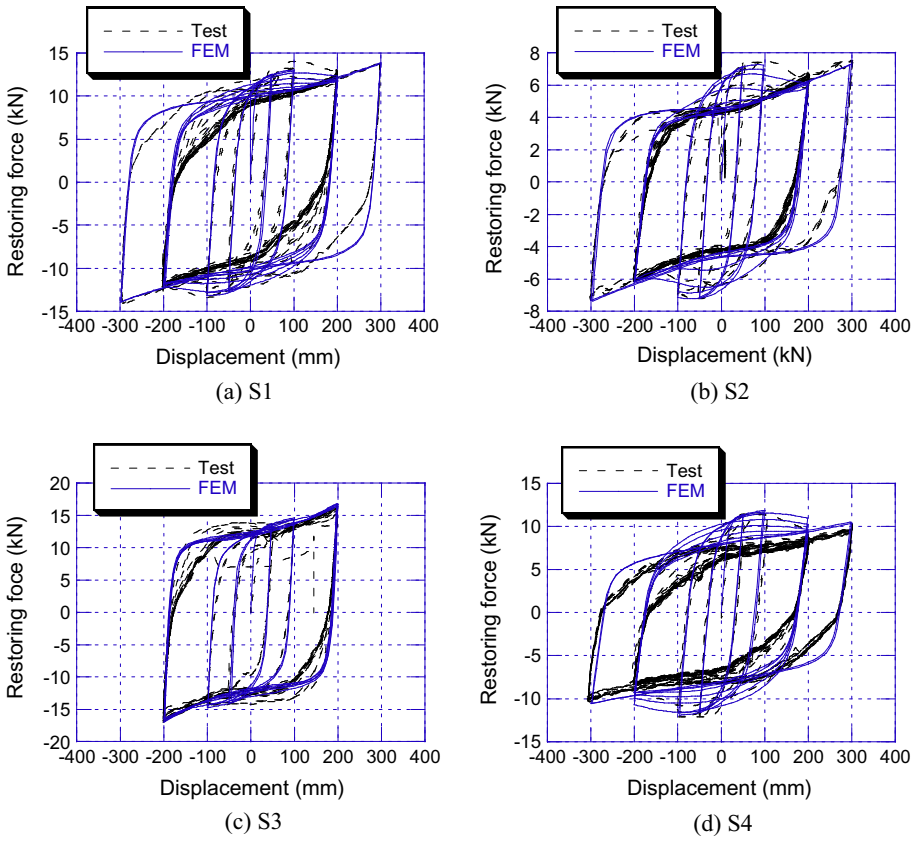

Fig. 9. Comparisons between FEM to physical test.

Table 3
Finite element analysis results.

No.	*ALLPD* (kN m)			$PEEQ_{max}$		
	FEM	Test	Error (%)	Bi-directional	Out-of-plane unidirectional	Ratio
S1	52.88	49.94	5.89	3.233	2.174	1.487
S2	25.81	24.72	4.41	2.738	1.638	1.672
S3	68.11	65.14	4.56	2.199	2.004	1.097
S4	40.78	37.47	8.83	2.174	1.680	1.294

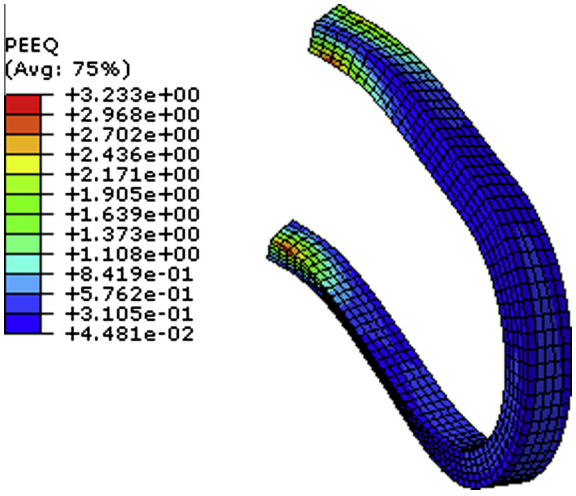

Fig. 10. *PEEQ* distribution of S1.

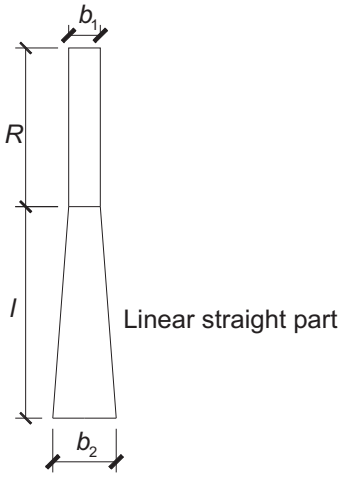

Fig. 11. Optimization approaches.

6. Optimization process

The parameters for the first-optimization level are shown in Table 4 and there were 15 models in the first level process. A wide range was assumed as the primary design space. l varied from 200 mm to 400 mm with an interval of 50 mm. b_2 varied from 40 mm to 60 mm with an interval of 10 mm. The finite element analyses were performed using ABAQUS. The loading scheme was the same as described in the section on the "Finite element model". Fig. 13(a) presents the results of the FE analyses. It can be seen that when b_c equals 50 mm the total energy dissipation capacity of the

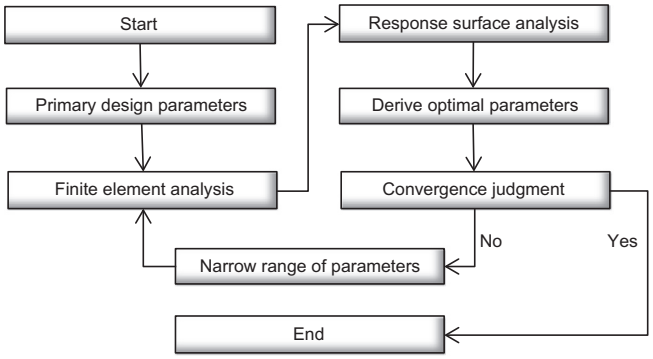

Fig. 12. Flowchart of optimization process.

Table 4
Models in optimization process.

b_c (mm)	l (mm)	Total model
40, 50, 60	200, 250, 300, 350, 400	15

U-shaped damper does not vary significantly with the length of the straight part. When b_c equaled 40 mm or 60 mm the total energy dissipation capacity increased with the length of the straight part and was obviously smaller than for the damper with b_c equal to 50 mm. The max $ALLPD/PEEQ^{0.6}_{max}$ was 87.304 kN m. The results for the regression analysis of the 15 models were obtained using MATLAB [29]. The least squares method was used in the regression analysis. The regression equation is as follows:

$$ALLPD/PEEQ^{0.6}_{max} = -486.7 + 247.9x + 653.3y + 29.1x^2 - 190.2y^2 - 266.7xy - 41.08x^2y + 79.66xy^2 + 10.01x^2y^2 \quad (10)$$

The R-square of the regression analysis was 0.9892, which indicated a large proportion of variance was accounted for by the equation [29]. The maximum residual error was no more than 1.097 kN m, showing the credibility of Eq. (10). The response surface for the first optimization level is shown in Fig. 13(b). The optimal design parameters were 312 mm and 51 mm for l and b_2 respectively.

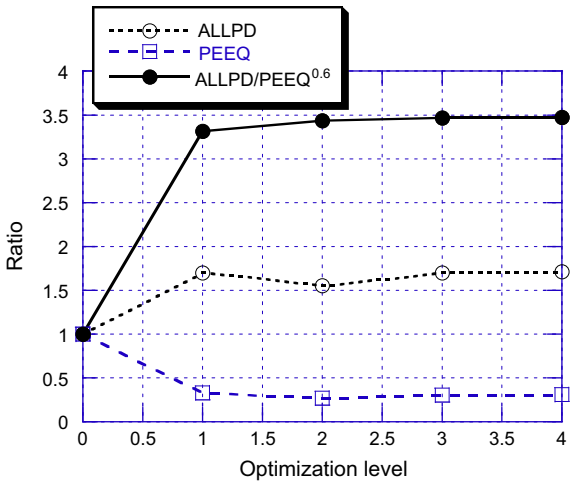

Fig. 14. Ratios for *ALLPD*, *PEEQ* and $ALLPD/PEEQ^{0.6}$.

Based on the results of the first-level optimization process the design space for the second-level optimization process was determined. l varied from 290 mm to 330 mm with an interval of 10 mm. b_2 varied from 46 mm to 56 mm with an interval of 5 mm. Finite element analyses were conducted in ABAQUS. The maximum $ALLPD/PEEQ^{0.6}_{max}$ was 89.77 kN m. The response surface was obtained based on the results of the second-level optimization process. The optimal parameters of second-level optimization were finally derived. The same processes were completed for the third-level and forth-level optimization processes. Table 5 shows the data for each-level optimization process.

The maximum $ALLPD/PEEQ^{0.6}_{max}$ for the third-level and the fourth-level optimization processes were very close. The optimal values of l and b_2 converged to 255 mm and 45 mm respectively. Further optimization processes were not necessary. S1 was the original specimen. The normalized *ALLPD*, maximum *PEEQ* and

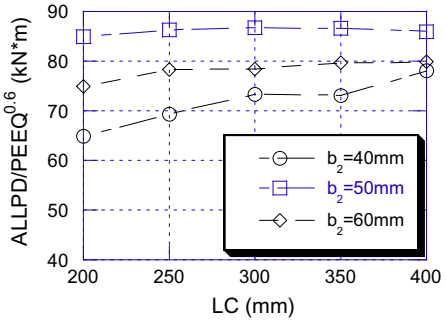

(a) Results of the FEM analysis

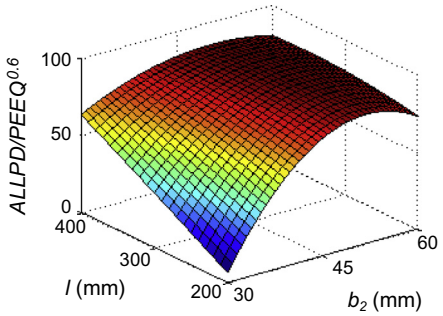

(b) Response surface

Fig. 13. Response surface for first-level optimization.

Table 5
Data of each level optimization.

Opt. level	l (mm)	b_c (mm)	Max $ALLPD/PEEQ^{0.6}_{max}$	Opt. l, b_c
1	200, 250, 300, 350, 400	40, 50, 60	86.76	312, 51
2	290, 310, 330	46, 51, 56	89.77	270, 45
3	260, 270, 280	42, 45, 48	90.69	261, 45.8
4	250, 255, 260	44, 45, 46	90.84	255, 46.6

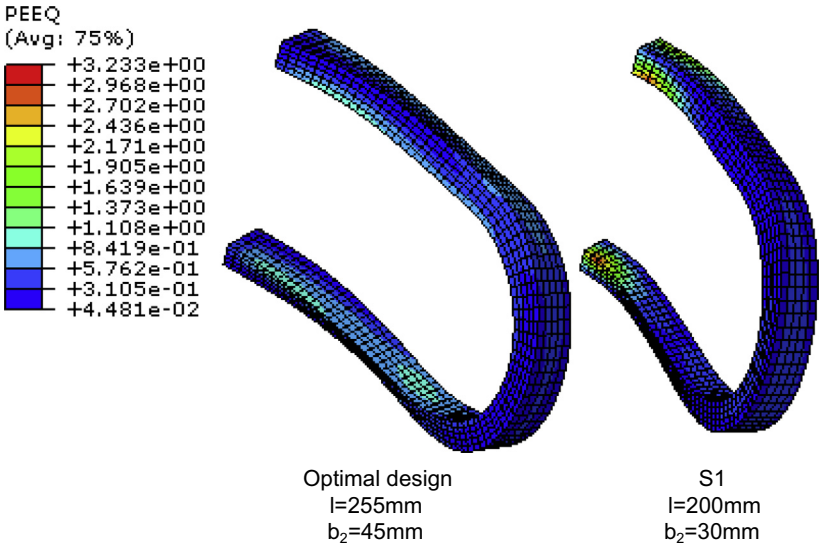

Fig. 15. Comparison on *PEEQ* distribution.

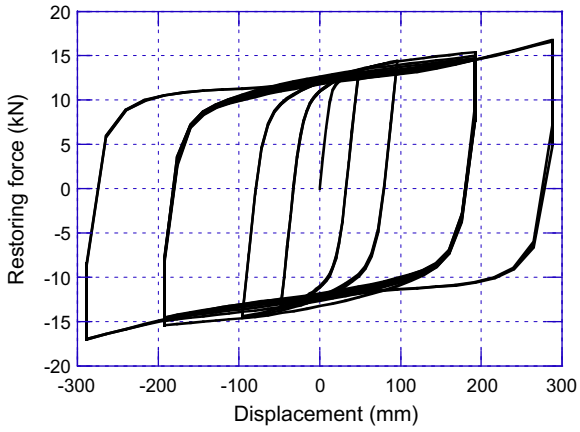

Fig. 16. Hysteresis curve of optimally design specimen.

$ALLPD/PEEQ^{0.6}_{max}$ of the optimal specimen of each level are shown in Fig. 14. After the optimization process the *ALLPD* increases to 90.572 kN m which is about 171% of S1. The maximum *PEEQ* decreased to 0.995 which was 30.7% of the value of S1. The $ALLPD/PEEQ^{0.6}_{max}$ of the optimized U-shaped damper was 90.84 kN m. The plastic strain distribution for the optimized damper is shown in Fig. 15. The *PEEQ* of the U-shaped damper distributed evenly along the straight part and the residual deformation was obviously smaller than that of S1. The decrease of the residual deformation is due to the uniform distribution of the equivalent plastic strain. The *PEEQ* at the end of the straight part reduced to about 0.4. The hysteresis curve for the optimal design specimen is shown in Fig. 16. There is no obvious decrease in the restoring force within the first six cycles of loading at an amplitude of 200 mm. Overall, the superior performance of the optimal design is mainly due to reduction of concentration of the plastic strain. The bi-directional performance of the U-shaped damper was significantly improved. It should be noticed that the optimal shape of the U-shaped damper for bi-directional deformation is not necessarily the optimal shape for other load conditions. The objective of the shape optimization is to control the strong nonlinearity of the U-shaped damper and alleviate the concentration of the plastic strain for bi-directional deformation. The behavior of the conventional U-shaped damper for unidirectional deformation is quite stable. The optimal U-shaped damper is overall similar to the conventional U-shaped damper, thus it is expected to have stable behavior under unidirectional deformation.

7. Conclusions

This study focused on the bi-directional performance of a U-shaped damper. The experimental study was first carried out on four specimens. The results for the physical test show that the strong geometric nonlinearity of the U-shaped damper under bi-directional loading led to a concentration of the plastic strain. A sophisticated finite element model was built in ABAQUS, and could simulate the mechanical behaviors of the specimens. Shape optimization of U-shaped damper was conducted in ABAQUS. The response surface method and regression analysis were used to obtain the optimal design parameters. Within the four level optimization process the optimal shape parameters were derived. The main conclusions obtained in the study are as follows:

(1) The conventional U-shaped damper presented a strong geometric nonlinearity under bi-directional loading, leading to the concentration of the plastic strain. The low cycle performance of the U-shaped damper under bi-directional loading was not as good as that under unique directional loading. The maximum *PEEQ* of the U-shaped damper under bi-directional deformation is 1.09–1.67 times of that under out-of-plane unidirectional deformation.
(2) A finite element model considering the kinematic hardening was built in ABAQUS. The comparisons between the results obtained from the finite element analyses with those from the physical tests demonstrated the effectiveness of the FE model of the U-shaped damper.
(3) The response surface method and regression analysis were used in the shape optimization process. Optimal design parameters were derived after the fourth optimization level. The results for the optimally designed U-shaped damper shows significant improvement compared to the conventional U-shaped damper.

Acknowledgements

Financial support by the Natural Science Foundation of China under Grant Nos. 51178250 and 51261120377, and Tsinghua University of China under Grant No. 2010Z01001, are gratefully acknowledged.

References

[1] Skinner RI, Kelly JM, Heine AJ. Hysteretic dampers for earthquake-resistant structures. Earthquake Eng Struct Dynam 1974;3(3):287–96.
[2] Martínez CA, Curadelli O, Compagnoni ME. Optimal placement of nonlinear hysteretic dampers on planar structures under seismic excitation. Eng Struct 2014;65:89–98.
[3] Pan P, Ye LP, Shi W, et al. Engineering practice of seismic isolation and energy dissipation structures in China. Sci China Technol Sci 2012;55(11):3036–46.
[4] Tabatabaei SAR, Mirghaderi SR, Hosseini A. Experimental and numerical developing of reduced length buckling-restrained braces. Eng Struct 2014;77:143–60.
[5] Soong TT, Spencer Jr BF. Supplemental energy dissipation: state-of-the-art and state-of-the-practice. Eng Struct 2002;24(3):243–59.
[6] Briones B, de la Llera JC. Analysis, design and testing of an hourglass-shaped copper energy dissipation device. Eng Struct 2014;79:309–21.
[7] Brando G, De Matteis G. Design of low strength-high hardening metal multi-stiffened shear plates. Eng Struct 2014;60:2–10.
[8] Sato E, Furukawa S, Kakehi A, et al. Full-scale shaking table test for examination of safety and functionality of base-isolated medical facilities. Earthquake Eng Struct Dynam 2011;40(13):1435–53.
[9] Kishiki Shoichi, Ohkawara Yuta, Yamada Satoshi, Wada Akira. Experimental evaluation of cyclic deformation capacity of u-shaped steel dampers for base-isolated structures. J Struct Constr Eng 2008;624:333–40.
[10] Chung YL, Nagae T, Hitaka T, et al. Seismic resistance capacity of high-rise buildings subjected to long-period ground motions: E-Defense shaking table test. J Struct Eng 2010;136(6):637–44.
[11] Kato S, Kim YB. A finite element parametric study on the mechanical properties of J-shaped steel hysteresis devices. J Constr Steel Res 2006;62(8):802–11.
[12] Deng K, Pan P, Wang C. Development of crawler steel damper for bridges. J Constr Steel Res 2013;85:140–50.
[13] Oh SH, Song SH, Lee SH, et al. Experimental study of seismic performance of base-isolated frames with U-shaped hysteretic energy-dissipating devices. Eng Struct 2013;56:2014–27.
[14] Koetaka Y, Chusilp P, Zhang Z, et al. Mechanical property of beam-to-column moment connection with hysteretic dampers for column weak axis. Eng Struct 2005;27(1):109–17.
[15] Tagawa H, Gao J. Evaluation of vibration control system with U-dampers based on quasi-linear motion mechanism. J Constr Steel Res 2012;70:213–25.
[16] Maleki S, Bagheri S. Pipe damper, Part I: experimental and analytical study. J Constr Steel Res 2010;66(8):1088–95.
[17] Pan P, Lam A, Lin X, et al. Cyclic loading tests and finite element analyses on performance of ring beam connections. Eng Struct 2013;56:682–90.
[18] Pan P, Tomofuji H, Wang T, et al. Development of peer-to-peer (P2P) internet online hybrid test system. Earthquake Eng Struct Dynam 2006;35(7):867–90.
[19] Ohsaki M, Tagawa H, Pan P. Shape optimization of reduced beam section under cyclic loads. J Constr Steel Res 2009;65(7):1511–9.
[20] Pan P, Ohsaki M, Tagawa H. Shape optimization of H-beam flange for maximum plastic energy dissipation. J Struct Eng 2007;133(8):1176–9.
[21] Liu Y, Shimoda M. Shape optimization of shear panel damper for improving the deformation ability under cyclic loading. Struct Multidisciplinary Optimization 2013:1–9.
[22] Sonmez M, Aydin E, Karabork T. Using an artificial bee colony algorithm for the optimal placement of viscous dampers in planar building frames. Struct Multidisciplinary Optimization 2013:1–15.
[23] Models for metals subjected to cyclic loading, Section 20.2.2 of the Abaqus Analysis User's Manual. ABAQUS 6.11. Dassault Systemes. Inc. 2010.
[24] Manson SS. Discussion. Trans ASME 1962;84:537–41.
[25] Coffin Jr LF. A study of the effects of cyclic thermal stresses on a ductile metal. Trans ASME 1954;76:931–50.
[26] Zhang Chaofeng, Zhang Zhisheng, Zhang Qiuju. Static and dynamic cyclic performance of a low-yield-strength steel shear panel damper. J Constr Steel Res 2012;79:159–203.
[27] Kanaji H, Hamada N, Ishibashi T, et al. Design and performance tests of buckling restrained braces for seismic retrofit of a long-span bridge. In :21th US–Japan bridge engineering workshop. Panel on wind and seismic effects; 2005.
[28] Dusicka P, Itani AM, Buckle IG. Cyclic response of plate steels under large inelastic strains. J Constr Steel Res 2007;63(2):156–64.
[29] Curve fitting Toolbox User's Guide. Mathworks Inc; 2010.